J Mater Sci (2007) 42:9005–9014
DOI 10.1007/s10853-007-1936-8

The structural efficiency of orthotropic stalks, stems and tubes

Ulrike G. K. Wegst · Michael F. Ashby

Received: 31 January 2007 / Accepted: 12 June 2007 / Published online: 7 August 2007

Abstract An optimised structure is one which uses the smallest quantity of the best material to perform its function, with adequate safety factor or margin for error. Structural optimisation occurs not only in mechanical engineering, but also in nature: plants with hollow stems or stalks gain a height advantage, and are thus more efficient, by approaching the optimum shape. Here we consider the optimisation of orthotropic tubes, typifying, in a mechanical sense, stalk and stem. The stiffness and strength of orthotropic tubes of initially circular section are reviewed, and diagrams are proposed which allow the optimum section shape to be selected.

Introduction

In creating structures to carry loads, hollow, thin-walled sections can be more efficient than thick-walled or solid ones. They use less material and are therefore lighter (more "economical") while resisting the same bending or torsional load; and this is true whether the design is based on stiffness or on strength. When the mode of loading is bending and the direction of loading is unknown, *circular tubes* are better than other shapes. And if nature is to act as a guide, circular tubes which are *orthotropic* are better than those that are isotropic using the same amount of material. An orthotropic tube is one in which the modulus and strength parallel to the tube axis differ from those in the circumferential direction; if this difference is chosen properly, the orthotropic tube is both stiffer and stronger in bending than the equivalent isotropic one. Orthotropic tubes are exploited both by engineers (composites, highly-drawn metals) and by nature (stalks, stems, bamboo culms) and are almost invariably structured so that the stiff, strong direction lies parallel to the axis of the tube. The question we address here is this: how can the tube shape (that is, the ratio of wall-thickness to tube radius) and the anisotropy ratio (ratio of axial to radial modulus and strength) be optimised to maximise the performance?

To answer this requires a study of the potential failure modes of the tube. When a tube is bent, its section tends to ovalise, loosing stiffness. Bent far enough, it fails in *mode 1*: ovalising and kinking with catastrophic stiffness loss—like a plastic drinking straw, bent until it collapses. But bending also creates tensile and compressive stresses in the tube wall; if either of these exceeds the uniaxial strength of the tube wall, the tube fails in *mode 2*: tensile yield or fracture, or compressive collapse—like a stick of celery, bent until it snaps. Finally, ovalisation has another, subtler, consequence: it creates circumferential stresses in the tube wall which, if they exceed the circumferential strength (almost always the lower one), cause *mode 3* failure: longitudinal splitting—like a stick of celery, pinched between the fingers.

Observations and analyses of the bending response of thin-walled orthotropic tubes appear in two quite separate bodies of literature. That relating to plant stems and stalks is largely experimental [1–14]. That focusing on light-weight engineering structures, and particularly on polymer-composite tubes are predominantly analytical, and generally treat only one aspect of what is a multi-faceted problem [15–26]. Only one paper [27] attempts, as we do

U. G. K. Wegst (✉)
Department of Materials Science and Engineering, Drexel University, 3141 Chestnut Street, Philadelphia, PA 19104, USA
e-mail: uwegst@coe.drexel.edu

M. F. Ashby
Department of Engineering, Cambridge University, Trumpington Street, Cambridge CB2 1PZ, UK

here, a comprehensive survey of competing failure modes and explores how well plants—particularly bamboo—are structured to combat them. We now review the stiffness and strength of thin-walled orthotropic tubes in more detail, allowing for ovalisation during bending and for four distinct failure modes. Much of the analysis closely parallels that of [27] and will therefore be kept brief. The recasting of all of the results in terms of section area and shape, and the novel construction and optimisation, both of shape and of anisotropy this allows, are new.

Bending of thin-walled orthotropic tubes

In designing a thin-walled tube to carry bending moments, two sets of consideration arise. The first set relates to *stiffness*, the second to the *collapse moment* (or *strength*).

Stiffness, ovalisation and the Brazier moment for orthotropic tubes

The curvature, C, of an elastically isotropic beam is related to the bending moment, M, which it carries by

$$M = IEC \tag{1}$$

where E is the Young's modulus of the material of which the beam is made and I is its second moment of area. We focus on a beam which is a thin-walled tube of initial radius, r, and wall-thickness, t, with cross-section $A = 2\pi rt$. If the bending is slight, the cross-section remains circular, when

$$I = \pi r^3 t \tag{2}$$

Then the moment is related to the curvature by

$$M = \pi r^3 tEC \tag{3}$$

and the elastic strain energy per unit length of the tube is

$$U = \frac{1}{2}\pi r^3 tEC^2 \tag{4}$$

However, if the bending is substantial, the tensile and compressive stresses in the tube walls due to its longitudinal curvature cause the cross-section to ovalise as in Fig. 1, and this has several consequences. The ovalisation reduces the second moment of area, I; further bending causes the ovalisation to increase and the stiffness to decrease, until a maximum bending moment, the Brazier moment, is reached and catastrophic failure follows [28]. In practice tubes fail at bending moments which are a little less than this because local defects trigger a local buckling mode, but we shall ignore this and identify the elastic collapse moment with the Brazier moment.

To find it, we follow the method and notation of [29]. Ovalisation is measured by ζ, the "cross-sectional shape-change parameter" (Fig. 1):

$$\varsigma = \frac{r-a}{r} \tag{5}$$

where r and a are the radius of the original circular shape and the minor axis of the ellipse respectively.

Then the total strain energy per unit length, U, of an isotropic tube which has been deformed into an arc of curvature C, replacing Eq. 4, becomes

$$U = \frac{1}{2}\pi r^3 tEC^2\left(1 - \frac{3}{2}\varsigma + \left[\frac{5}{8}\varsigma^2\right]\right) + \frac{3}{8}\frac{\pi t^3}{r}\varsigma^2 E \tag{6}$$

The first term of the right hand side of this equation describes the strain energy due to longitudinal stretching, the second that due to ovalisation (circumferential bending).

For an orthotropic material this expression is modified by replacing E with the longitudinal modulus, $E_{||}$, in the longitudinal stretching term and with the transverse modulus, $E_{\perp}$, in the ovalisation term.

$$U = \frac{1}{2}\pi r^3 tE_{||}C^2\left(1 - \frac{3}{2}\varsigma + \left[\frac{5}{8}\varsigma^2\right]\right) + \frac{3}{8}\frac{\pi t^3}{r}\varsigma^2 E_{\perp} \tag{7}$$

Omitting the ζ^2 term enclosed in square brackets (justified in a moment), we seek the ovalisation, ζ, for a given curvature, C, which minimises the total energy, U. Setting $\delta U/\delta\zeta = 0$ leads to

$$\varsigma = \frac{r^4}{t^2}\left(\frac{E_{||}}{E_{\perp}}\right)C^2 = \frac{4}{3}c^2 \tag{8}$$

where the dimensionless curvature, c, is defined by

$$c^2 = \frac{3}{4}\frac{r^4}{t^2}\left(\frac{E_{||}}{E_{\perp}}\right)C^2 \tag{9}$$

Substituting Eqs. 8 and 9 (inverted) for ζ and C^2 in Eq. 7, gives the strain energy, U, as a function of c alone

$$U = \frac{2\pi}{3}\frac{t^3}{r}E_{\perp}\left(c^2 - c^4\right) \tag{10}$$

From this we calculate the bending moment, $M = \frac{c}{C}\frac{dU}{dc}$, as

$$M = \frac{2\pi}{\sqrt{3}}rt^2\left(E_{||}E_{\perp}\right)^{1/2}\left(c - 2c^3\right) \tag{11}$$

Equation 11 is the generalisation of the simple Eq. 3 for orthotropic tubes, including the effect of ovalisation, and

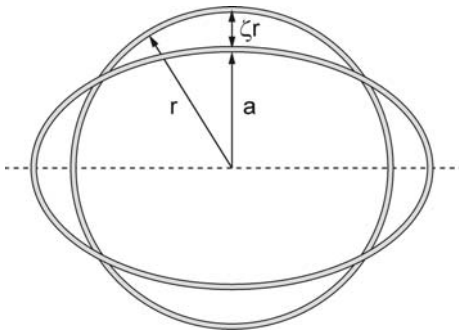

Fig. 1 Schematic representation of the ovalisation of a tube loaded in bending. The radius of the original circular cross-section is r_0 and the minor axis of the ovalised section is a

reduces to it when $E_{||} = E_{\perp}$ and $c \ll 1$. The maximum M—the Brazier moment M_B—is found by setting the differential of Eq. 11 with respect to C equal to zero

$$\frac{dM}{dC} = \frac{dM}{dc}\frac{c}{C} = 0 \tag{12}$$

giving the critical value $c = 1/\sqrt{6}$ which, when reinserted into Eq. 11 gives:

$$M_B = \frac{2\sqrt{2}}{9}\pi r t^2 \left(E_{||}E_{\perp}\right)^{1/2} \tag{13}$$

Strategies exist for suppressing ovalisation. Bamboo culm (to take an example from nature) is an orthotropic tube which is divided into chambers by stiff diaphragms which are positioned at the nodes from which the leaves grow. It has been considered [1, 4, 9, 11, 27, 30–33] that these might act as ring stiffeners, suppressing ovalisation. The isotropic tube with periodic stiffeners is well treated in the mechanics literature (see for example [29, 34]).

Consider a tube of finite length, L, thickness, t, and radius, r, which is fitted with end-pieces which preserve the original circular shape (thus L becomes the stiffener spacing or internode length, as in Fig. 2a). Calladine [29] derives the dimensionless group

$$\Omega = \left(\frac{tL^2}{r^3}\right)^{1/2} \tag{14}$$

which characterises the problem: if $\Omega < 0.5$, ovalisation is largely suppressed, stiffening the tube and local buckling occurs when the critical stress is reached to cause axisymmetric buckling under uniaxial compression on the compressive face of the tube [35]; for $0.5 < \Omega < 2$, ovalisation at the point of local buckling increases with an increase in Ω and the critical moment decreases until at $\Omega \geq 2$ it is approximately equal to that at failure of an infinitely long tube. Thus for $\Omega > 0.5$ the end-pieces or diaphragms have little influence.

Orthotropy changes this. A high value of the circumferential modulus $E_{\perp}$ makes ovalisation difficult; a low value makes it easy. A tube for which $E_{||}/E_{\perp} > 1$ ovalises more, for the same curvature C, than one for which the opposite is true; to prevent the ovalisation becoming critical, the stiffeners must be placed closer together. Suo [36, 37] introduces an orthotropic scaling factor, the anisotropy ratio, ξ, which takes account of this phenomenon

$$\xi = \frac{E_{||}}{E_{\perp}} \tag{15}$$

With it, the effective length, λ, of the internode can be calculated

$$\lambda = \xi^{1/4} L = \left(\frac{E_{||}}{E_{\perp}}\right)^{1/4} L \tag{16}$$

and the expression for Ω for an orthotropic tube becomes

$$\Omega = \left(\frac{t\lambda^2}{r^3}\right)^{1/2} = \left(\frac{E_{||}}{E_{\perp}}\right)^{1/4}\left(\frac{tL^2}{r^3}\right)^{1/2} \tag{17}$$

with the same limit ($\Omega < 0.5$) required to suppress ovalisation. In plants a typical anisotropy ratio ξ is 10 [38]. Taking this value, the effective length of an internode is increased by a factor of 1.8 so that the ovalisation even of relatively short internodes with either $L/r = 1.7$ and $r/t = 6$ or with $L/r = 1$ and $r/t = 2$ cannot be prevented.

A second scheme—one seen in many plant stems—is that of filling the tube with a foam (Fig. 2b). A low-density foam is effective in suppressing local buckling [39, 40], which is a bifurcation, but less so in suppressing ovalisation, which is not. But since local buckling occurs before the Brazier moment is reached, foam-filling provides a way of raising the failure moment without greatly increasing the mass.

A third strategy—one seen in bone, particularly that of birds—is to insert a network of transverse struts, forcing the tube to remain circular, until the struts fail. Provided the struts are separated by no more than a few tube-radii they can, like the ring-stiffeners, successfully suppress ovalisation.

Suppressing ovalisation is important: not only does it increase the bending stiffness of the tube, but it also inhibits two of the three failure modes discussed next.

Failure of thin-walled orthotropic tubes

The tube can fail in one of three ways.

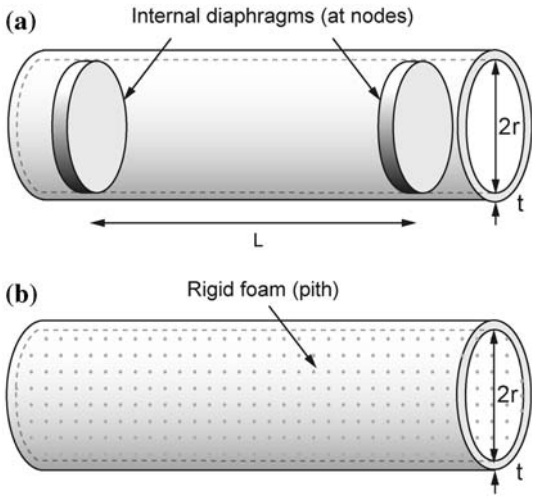

Fig. 2 Schematic showing suppression of ovalisation (**a**) by diaphragms and (**b**) by a foam core

Failure by ovalisation, instability and local kinking

This, as described above, occurs at a moment M_1 which is sufficiently close to the Brazier moment M_B (Eq. 13) curve that it can be approximated by this value:

$$M_1 = M_B \tag{18}$$

If the tube is loaded with a moment larger than this, a kink forms in the tube wall which leads to catastrophic failure by buckling.

Failure by tensile fracture or compressive collapse

The maximum stress, σ_{max}, in the wall of a thin-walled tube of radius r and thickness t with a second moment of area $I = \pi r^3 t$, loaded by a bending moment, M, is:

$$\sigma_{max} = \pm\frac{Mr}{I} = \pm\frac{M}{\pi r^2 t} \tag{19}$$

It is tensile on the side of the tube furthest from the centre of curvature, and compressive on the other side. If the tensile stress exceeds the strength in tension of the material of which the wall is made, the tube will fracture. If, instead, the compressive stress exceeds the compressive collapse load of the tube wall, failure again follows. Both are treated by equating Eq. 19 to σ_f, where this is the tensile failure stress or the compressive collapse stress, whichever is smaller. Both natural and man-made orthotropic tubes are, very frequently, composites with fibres which lie predominantly parallel to the tube axis. Such structures fail in compression by fibre buckling at a stress which is lower than the tensile strength, and for this reason we will for the moment identify σ_f with the compressive failure strength parallel to the tube axis, $\sigma_{c||}$, giving:

$$M_2 = \pi r^2 t \sigma_{c||} \tag{20}$$

Failure by longitudinal splitting

The last failure mode is a little harder to analyse. A consequence of a fibre lay-up which increases longitudinal stiffness and strength is that the transverse properties suffer. In particular, the transverse tensile strength (which we shall call $\sigma_{t\perp}$) of near-uniaxial fibre composites can be so low that the tube, when bent, splits along its length. The tensile stress which causes this arises from the ovalisation, as sketched in Fig. 3: it is greatest on the inner surface of the tube at the point A and on the outer one at B. It is calculated by imagining that ovalisation is caused by two point forces, W, which generate a moment M^* at B [41], where

$$M^* = 0.18 \cdot Wr \tag{21}$$

The point loads also lead to an ovalisation of the cross-section [41] with a change in vertical diameter D_v, which we describe by the dimensionless cross-sectional shape-change parameter as before

$$\varsigma = \frac{D_v}{2r} = \frac{0.149 \cdot Wr^3}{2rEI} = 0.89 \cdot \frac{Wr^2}{E_\perp t^3} \tag{22}$$

Neglecting the small additional compressive stresses, $W/2t$, which are due to the point loads, we find that the maximum circumferential stress is related to the bending moment by

$$M^* = \frac{1}{6}\sigma_{\perp max} t^2 \tag{23}$$

Rearranging and substituting Eq. 22 for Wr in Eq. 21 and equating the result with Eq. 23 yields a correlation between the maximum transverse stress in the tube wall and the ovalisation

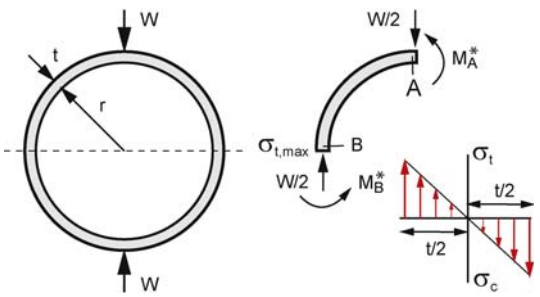

Fig. 3 Schematic of a bamboo cross-section, illustrating the way in which the tensile stress which causes splitting is calculated

$$\varsigma = 0.82 \cdot \frac{\sigma_{\perp \max}}{E_\perp} \frac{r}{t} \tag{24}$$

The final step is to link the ovalisation to the curvature which is its real origin. Equating this expression for the ovalisation with the one we obtained in the buckling analysis above (Eq. 8) we find a correlation between the maximum transverse stress, $\sigma_{\max}$, and the dimensionless curvature

$$c = \left(0.62 \cdot \frac{\sigma_{\perp \max}}{E_\perp} \frac{r}{t}\right)^{1/2} \tag{25}$$

Equating $\sigma_{\perp \max}$ with the transverse tensile strength of the tube wall, $\sigma_{t\perp}$, and substituting Eq. 25 for c in Eq. 11 we find a new general expression for the bending moment for longitudinal splitting of the tube:

$$M_3 = 2.86 \cdot (rt)^{3/2} \left(E_{||} \sigma_{t\perp}\right)^{1/2} \left[1 - 1.24 \left(\frac{r}{t} \frac{\sigma_{t\perp}}{E_\perp}\right)\right] \tag{26}$$

As expected, M_3 decreases as the transverse strength, $\sigma_{t\perp}$, decreases.

Optimisation of shape and anisotropy: failure maps

Failure mechanisms compete. The dominant mechanism is the one which occurs first as the bending moment M on the tube is progressively increased; this usually means that it is the one with the lowest value of the failure moment $(M_1, M_2, M_3, \textit{etc.})$, though there is one exception. We now explore this competition, seeking first the optimum shape for the tube, then the optimum anisotropy ratio. To do so, we express the geometric variables (contained in I) in such a way as to separate *section-area*

$$A = 2\pi rt \tag{27}$$

from *section-shape* characterised by the *shape factor*, ϕ:

$$\phi = \frac{4\pi I}{A^2} = \frac{r}{t} \tag{28}$$

The shape factor ϕ is dimensionless; beams with the same ϕ have cross-sections which may differ in size, but have the same proportions: their cross-sections look like photographic reductions or enlargements of each other. The form of the expressions for the failure moments M_1, M_2 and M_3 suggests a plot of $M/A^{3/2}$ (with units of GPa) against the shape factor, $\phi = r/t$, to examine the competition in failure modes. (Dividing the moment by $A^{3/2}$ ensures that we are comparing tubes of similar cross-sectional area and same mass per unit length.)

Rearranging Eq. 18 (with (13)) give an expression for failure by buckling:

$$\frac{M_1}{A^{3/2}} = \frac{1}{9\sqrt{\pi}} \left(\frac{E_{||} E_\perp}{\phi}\right)^{1/2} \tag{29}$$

That for tensile failure/compressive collapse (Eq. 20) now reads:

$$\frac{M_2}{A^{3/2}} = \frac{1}{\sqrt{8\pi}} \sigma_{c||} \phi^{1/2} \tag{30}$$

and that for splitting (Eq. 26) becomes:

$$\frac{M_3}{A^{3/2}} = 0.18 \cdot \left(\sigma_{t\perp} E_{||}\right)^{1/2} \left[1 - 1.24 \left(\frac{\sigma_{t\perp}}{E_\perp} \phi\right)\right] \tag{31}$$

Failure maps

Figure 3 shows the construction of a *failure map* for orthotropic tubes without stiffeners, loaded in bending. Three curves are plotted in Fig. 4a, corresponding to each of the three failure modes: buckling (Eq. 29), fracture/yield (Eq. 30), and splitting (Eq. 31).

The overall failure moment of the tube is defined by the lower envelope of these curves, with one qualification, detailed below. A change of mechanism takes place where the curves intersect—that is, at the points **A, B** and **C**. The first of these occurs at the value of ϕ at which failure by fracture/yield—Eq. 30—and by splitting—Eq. 31—have the same value of $M/A^{3/2}$. The failure map of Fig. 4c illustrates that the point **A** lies well to the left of the downward-curving segment of the M_3 curve, which is caused by the term in square brackets in Eq. 31. Neglecting this term, equating the two and solving for ϕ gives:

$$\phi_{\mathrm{A}} = 0.81 \cdot \left(\frac{\sigma_{t\perp} E_{||}}{\sigma_{c||}^2}\right) \tag{32}$$

(a full solution of ϕ_{A} is given in Appendix A). The second change of mechanism occurs at the value of ϕ at which buckling—Eq. 29—and fracture/yield—Eq. 30—have the same value of $M/A^{3/2}$. Equating these and solving for ϕ gives:

$$\phi_{\mathrm{B}} = 0.31 \cdot \frac{\left(E_{||} E_\perp\right)^{1/2}}{\sigma_{c||}} \tag{33}$$

However, since the splitting curve (Eq. 31) has the lowest values of $M/A^{3/2}$ for $\phi_{\mathrm{A}} < \phi < \phi_{\mathrm{C}}$ in Domain (2), failure occurs by splitting.

The situation in Domain (3) requires a little more explanation. At a first glance one might think that, as in

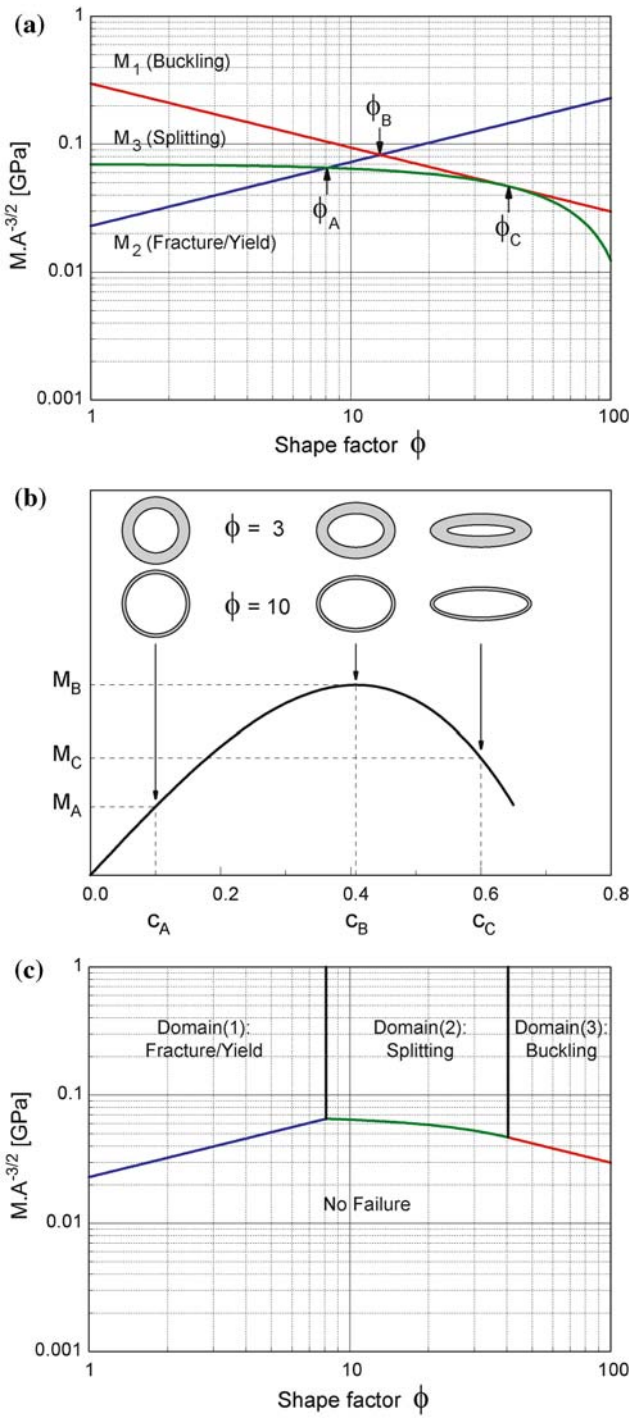

Fig. 4 (**a**) A failure map of loading coefficient $M/A^{3/2}$ plotted against the shape factor ϕ for the three failure curves M_1 (fracture/yield), M_2 (buckling) and M_3 (splitting). The intersections at I, II and III indicate the transitions from one failure mechanism to another. (**b**) A graph showing bending moment, M, plotted against dimensionless curvature, c. (**c**) A failure map showing the three failure domains fracture/yield (1), buckling (2) and splitting (3)

Domain (2), splitting determines the failure moment (since the lowermost curve is that of M_3), but this is not so. The peak moment in Domain (3) is set by the Brazier moment, not by splitting—although splitting may subsequently occur. Figure 3b helps to explain this: it is a graph showing the bending moment, M, plotted against dimensionless curvature, c, and illustrates the sequence of events. On bending, M increases with c until the Brazier moment, M_B, is reached, beyond which it decreases. For values of ϕ less than ϕ_C, the condition for splitting is met before the Brazier moment is reached, and splitting therefore determines the failure moment in Domain (2). But for values of ϕ greater than ϕ_C, the tube is so thin-walled that the Brazier moment is reached first, before the stresses in the tube wall are large enough to cause splitting. Thus the tube then buckles, and splitting, if it occurs at all, is a secondary event. The transition occurs at the value of ϕ at which the M_3 is tangent to M_1, when, as shown in the development of Eq. 13, $c = 1/\sqrt{6}$ and, from Eq. 25 (with $r/t = \phi$ and $\sigma_{\perp\max} = \sigma_{t\perp}$)

$$\phi_C = 0.27 \cdot \left(\frac{E_\perp}{\sigma_{t\perp}}\right) \tag{34}$$

These boundary values of ϕ allow the failure map to be completed. The result is shown in Fig. 4c. It displays the fields of dominance of each failure mechanism. Failure maps are material-specific, that is, they are calculated for given sets of the four key material properties, $E_{||}$, $E_\perp$, $\sigma_{c||}$ and $\sigma_{t\perp}$; the values used for Fig. 4 are listed in Table 1.

Optimisation of shape

The best shape for the tube is that which—for a given cross-section A—carries the greatest moment M. We therefore seek the value of ϕ at which $M/A^{3/2}$ is a maximum. For the conditions of Fig. 4c the answer is simple: the best shape is that corresponding to ϕ_A, and since this lies well to the left of the downward-curving part of the M_3 curve, it is well approximated by Eq. 27.

There is another possibility. As $\sigma_{t\perp}$ increases, splitting becomes more difficult, the M_3 curve moves upwards and the "splitting" domain shrinks in size and finally disappears. At the point at which this happens

$$\phi_A = \phi_B \tag{35}$$

giving (by Eqs. 32 and 33) the condition for the transition to no-splitting as:

$$\frac{\sigma_{t\perp}}{\sigma_{c||}} = 0.38 \cdot \left(\frac{E_\perp}{E_{||}}\right)^{1/2} \tag{36}$$

When this condition is met, the shape which gives the largest value of $M/A^{3/2}$ is that corresponding to ϕ_B.

Table 1 Data used in plotting Figs. 3 and 5: Young's modulus parallel and perpendicular to the tube axis, compressive strength parallel to the tube axis and tensile strength perpendicular to the tube axis

	Young's Modulus		Compressive Strength	Tensile Strength
	(parallel) $E_{\|\|}$ [GPa]	(perpendicular) $E_{\perp}$ [GPa]	(parallel) $\sigma_{c\|\|}$ [MPa]	(perpendicular) $\sigma_{t\perp}$ [MPa]
Green				
Low	5	0.5	45	4
Medium	10	1	50	5
High	15	1.5	55	6
Dry				
Low	10	1	100	8
Medium	15	1.5	115	10
High	20	2	130	12

In the practice of engineering design, gradual or "benign" failure modes, such as yielding, are viewed with less alarm than those which are sudden or "catastrophic", among which are buckling and splitting. Responding to this, the designer applies a greater safety factor to catastrophic modes than to those which are benign, and there is some evidence (see below) that nature may do the same. The practical consequence of this is to shift the optimum shape a little to the left on Fig. 4c, that is, to slightly smaller values of ϕ.

Optimisation of anisotropy

The last section identified two expressions for the optimum shape, ϕ, for orthotropic tubes, expressed in terms of material properties. By substituting these back in the failure equations, the failure moment of a tube of optimum shape can be written as a function of material properties alone. If splitting is possible, (that is, Eq. 36 is *not* satisfied), the ideal shape is that corresponding to ϕ_A. Substituting this into Eq. 30 gives the optimum moment that can be achieved with a given set of material properties:

$$\frac{M_{opt}}{A^{3/2}} = 0.18 \cdot \left(\sigma_{t\perp} E_{||}\right)^{1/2} \quad \text{with } \phi_{opt} = 0.81 \cdot \left(\frac{\sigma_{t\perp} E_{||}}{\sigma_{c||}^2}\right) \tag{37}$$

If, on the other hand, splitting is suppressed (that is, Eq. 36 *is* satisfied), the ideal shape is that corresponding to ϕ_B. Substituting this into Eq. 30 gives

$$\frac{M_{opt}}{A^{3/2}} = 0.11 \cdot \left(\sigma_{c||}\left(E_{||}E_{\perp}\right)^{1/2}\right)^{1/2} \quad \text{with } \phi_{opt} = 0.31 \cdot \frac{\left(E_{||}E_{\perp}\right)^{1/2}}{\sigma_{c||}} \tag{38}$$

Many orthotropic materials are fibre-reinforced composites, and for these a degree of control of the anisotropy is possible by adjusting the lay-up. It is then reasonable to ask: what is the best value for the anisotropy? To answer this, consider an idealised example: that of a tube made of fibres of modulus E_f and strength σ_f, in a matrix of modulus E_m and strength σ_m. Let a fraction γ of the total volume fraction of fibres, f, lie parallel to the tube axis; the remaining fraction $(1 - \gamma)$ is oriented circumferentially. Then, to an adequate approximation for illustrative purposes, the moduli of the material are:

$$\begin{aligned} E_{||} &= (1-f)\cdot E_m + \gamma \cdot f \cdot E_f \quad \text{and} \\ E_{\perp} &= (1-f)\cdot E_m + (1-\gamma)\cdot f \cdot E_f \end{aligned} \tag{39}$$

Defining $\bar{E}$ as the value of E for which $\gamma = 1/2$ (when the material is quasi-isotropic)

$$\bar{E} = (1-f)\cdot E_m + \frac{1}{2}\cdot f \cdot E_f \tag{40}$$

we find

$$\begin{aligned} E_{||} &= \bar{E}\left(1 + \left(\gamma - \frac{1}{2}\right) f \frac{E_f}{\bar{E}}\right) \quad \text{and} \\ E_{\perp} &= \bar{E}\left(1 + \left(\frac{1}{2} - \gamma\right) f \frac{E_f}{\bar{E}}\right) \end{aligned} \tag{41}$$

with similar expressions for the strengths in terms of the strength σ at $\varphi = 1/2$:

$$\begin{aligned} \sigma_{||} &= \bar{\sigma}\left(1 + \left(\gamma - \frac{1}{2}\right) f \frac{\sigma_f}{\bar{\sigma}}\right) \quad \text{and} \\ \sigma_{\perp} &= \bar{\sigma}\left(1 + \left(\frac{1}{2} - \gamma\right) f \frac{\sigma_f}{\bar{\sigma}}\right) \end{aligned} \tag{42}$$

We take, as an example, the case in which the optimum shape is limited by ϕ_B, when Eq. 38 applies. Substituting for $E_{||}$, $E_{\perp}$, and $\sigma_{c||}$ gives:

$$\frac{M_{opt}}{A^{3/2}} = 0.11(\bar{\sigma}\cdot\bar{E})^{1/2} \times \left\{\left(1+\left(\gamma-\frac{1}{2}\right)\beta\right)^{1/2} \times \left[\left(1+\left(\gamma-\frac{1}{2}\right)\alpha\right)\left(1+\left(\frac{1}{2}-\gamma\right)\alpha\right)\right]^{1/4}\right\} \quad (43)$$

with $\alpha = f\frac{E_f}{\bar{E}}$ and $\beta = f\frac{\sigma_f}{\bar{\sigma}}$.

The limits for α are determined for the extreme cases that $E_m \ll E_f$, when

$$\alpha = f\frac{E_f}{\bar{E}} = \frac{f\cdot E_f}{(1-f)\cdot E_m + \frac{1}{2}\cdot f\cdot E_f} \approx \frac{f\cdot E_f}{\frac{1}{2}\cdot f\cdot E_f} = 2 \quad (44)$$

and that $E_m = E_f/2$, when

$$\alpha = f\frac{E_f}{\bar{E}} = \frac{f\cdot E_f}{1/2\cdot\left[(1-f)E_f + f\cdot E_f\right]} = 2f \quad (45)$$

With typical values for the fibre-volume fraction $0 \le f \le 0.6$ and an analogous analysis for β, we find that $0 \le \alpha < 2$ and $0 \le \beta < 2$.

The term in the curly brackets of Eq. 43 describes the way in which the efficiency of material usage, measured by $M/A^{3/2}$, varies with the degree of anisotropy. When $\gamma = 1/2$, the material is isotropic and the bracketed term takes the value 1. When $\gamma = 1$ all the fibres are aligned parallel to the tube axis and anisotropy is maximised. Figure 5 shows this expression plotted against $\gamma\,(0.5 < \gamma < 1)$ for different values for α and β. Note that α and β will vary independently but in parallel. In the extreme case that the material contains no fibres and is truly homogeneous ($\alpha = \beta = 0$), the failure moment is, correctly, independent of the parameter γ. There is a broad maximum between $\gamma = 0.75$ and $\gamma = 1.0$, depending on the values of α and β, meaning that there is an "ideal" anisotropy that maximises the efficiency. To illustrate this with an example, we seek to optimise the fibre distribution of a composite tube with a 48% volume fraction of fibres with a Young's modulus ten times higher than that of the matrix. Assuming that also the fibre strength is ten times higher than that of the matrix, we calculate that $\alpha = \beta = 1.648$. With these values we find that the expression in the curly brackets in Eq. 43 reaches a maximum at $\gamma = 0.803$, thus when about 80% of the fibres are aligned with the longitudinal axis of the tube; giving an efficiency that is 14% larger than that of an isotropic tube.

With a more detailed model of how stiffness and strength depend on structure (here described by α, β and γ) a precise optimisation becomes possible, this is, however, beyond the scope of this study.

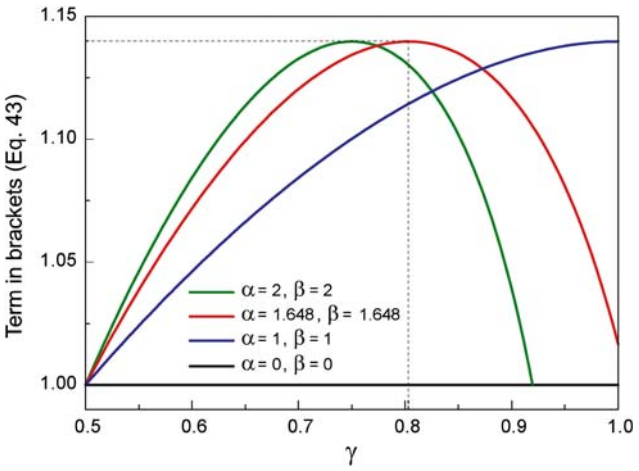

Fig. 5 The graph shows the expression in curly brackets ({}) of Eq. 43 plotted against γ for a number of different values for α and β. Note that α and β will vary independently but in parallel. In the extreme case that the material is truly homogeneous ($\alpha = \beta = 0$), the failure moment is, correctly, independent of the tubes shape (*black line*)

An application: bamboo culm

In Fig. 6a and b, failure curves are plotted for a typical range of green and dry bamboo culms. The three sets of lines on each chart describe culms with 'high', 'medium' and 'low' properties as listed in Table 1. In Fig. 6c the failure modes of a green bamboo culm (green lines) and a dry bamboo culm (red lines) both with medium properties are compared. We may now evaluate the stiffness requirement required by M_4 in Eq. A4, using typical shape factors, in the range $\phi = 2$–6. The shape factors and stiffness requirement circumscribe the region of the chart on which bamboo culms lie; it is plotted as a box. In all cases the failure moment increases with increasing ϕ up to the boundary between the 'fracture/yield' region and the 'splitting' regime; beyond this it slowly falls. The optimum shape is that at the peak.

From an engineering point of view, the most efficient shape for safe design is that which falls into the region just below the highest part of the fracture-domain (the peak of the fracture envelope). This ensures that catastrophic failure by local buckling and splitting is prevented while the material is used most efficiently. This is what we find for both the green and the dry bamboo.

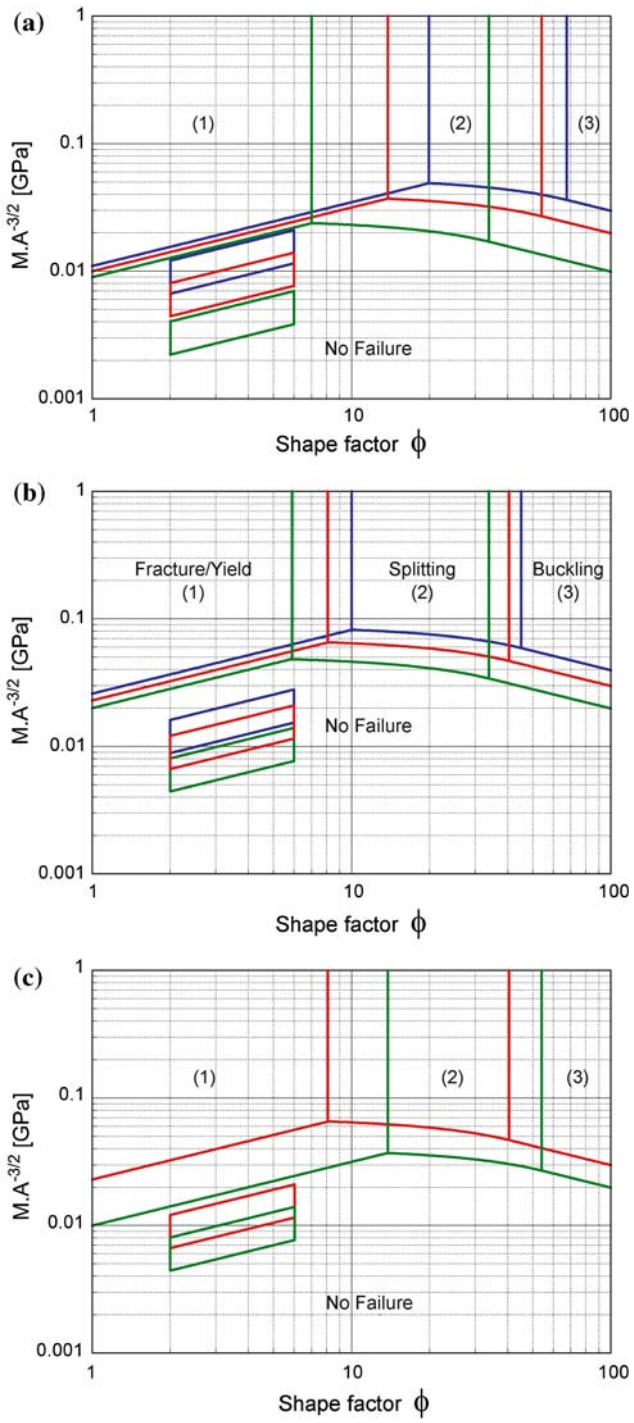

Fig. 6 (**a**) and (**b**) Failure maps plotting the loading coefficient $M/A^{3/2}$ against shape factor ϕ for typical green (**a**) and dry (**b**) bamboo culms. The green, blue and red sets of lines indicate low, medium and high property values as listed in Table 1. The boxes circumscribe the region in which bamboo typically lies according to its shape and the stiffness criterion. The numbers (1), (2) and (3) label the three failure domains fracture/yield, splitting and buckling, respectively. (**c**) A failure map comparing green (green lines) and dry (red lines) bamboo culms of medium material properties

Acknowledgements The ideas presented here have been helped by discussions with numerous colleagues and associates. We particularly wish to acknowledge the inputs and suggestions of Prof. C.R. Calladine, Dr. H. R. Shercliff, Dr. P. M. Weaver and of an anonymous reviewer. We also wish to acknowledge the support of the Royal Society of London and the US Advance Research Project Agency through the University Research Initiative under Office of Naval Research Contract No. N-00014092-J-1808.

Appendix 1 full solution for $\phi_{\mathbf{A}}$

The transition from fracture/yield to splitting is found by equating the respective moments of failure at **A**:

$$\phi_A = \frac{A}{2} \pm \left(\frac{A^2}{4} - B\right)^{1/2} \tag{A1}$$

with

$$A = \left[\frac{1 + 2.037 \cdot \left(\frac{E_{||}}{E_{\perp}}\right)\left(\frac{\sigma_{t\perp}}{\sigma_{c||}}\right)^2}{1.259 \cdot \left(\frac{\sigma_{t\perp}}{E_{\perp}}\right)^2 \left(\frac{E_{||}\sigma_{t\perp}}{\sigma_{c||}^2}\right)}\right] \quad \text{and B} = \left(\frac{1}{1.236}\right)^2 \left(\frac{E_{\perp}}{\sigma_{t\perp}}\right)^2$$

Appendix 2 failure through inadequate stiffness

The final criterion for the macroscopical mechanical performance is that of stiffness. Mosbrugger [42] classifies plants according to their structural behaviour: either the plant is a 'flexibility strategist' and reduces external loads by bending or it is a 'stability strategist' and has a structure which is stiff and strong enough to withstand the loads without much bending. As the principal load is that due to wind and the velocity of wind increases with height above ground, a flexible tree which bends in a strong wind reduces the moment arm of the net wind force, especially if elastic deformation of its crown reduces its down-wind profile. Tree trunks are frequently stability strategists, whereas their branches must be capable of bending to a quarter-circle. The curvature of the bamboo culm, C, can then be expressed as a function of the length, l, of the stem

$$C = \frac{1}{R} \approx \frac{\pi}{21} \tag{A2}$$

Substituting this expression for C in Eq. 8 and inserting the result for c in Eq. 13b gives the bending moment, M, which bends the stem into a quarter-circle

$$M = \frac{\sqrt{\pi}}{4\sqrt{2}}\left(\frac{r}{l}\right)A^{3/2}\phi^{1/2}E_{||}\left[1 - \frac{3\pi^2}{8}\left(\frac{r}{l}\right)^2\phi^2\left(\frac{E_{||}}{E_{\perp}}\right)\right] \tag{A3}$$

The second expression in the square bracket is very small due to the high slenderness ratios of bamboo ($\phi = l/r$ = 550–1000, [43]) and may therefore be neglected. The moment which bends a stem to a quarter-circle may therefore be rewritten as

$$M_4 = \frac{\sqrt{\pi}}{4\sqrt{2}}\left(\frac{r}{l}\right)A^{3/2}\phi^{1/2}E_{||} \quad \text{(A4)}$$

If the plant is to function as a flexibility strategist, it must be able to do this without failing by any of the other three mechanisms analysed above.

References

1. Amada S, Munekata T, Nagase Y, Ichikawa Y, Kirigai A, Yang ZF (1996) J Comp Mat 30:800
2. Arce-Villalobos OA (1993) Fundamentals of the design of bamboo structures. PhD Thesis, Eindhoven University of Technology, Netherlands
3. Niklas KJ (1989) Am J Bot 76:521
4. Niklas KJ (1992) Plant biomechanics: an engineering approach to plant form and function. University of Chicago Press, Chicago
5. Niklas KJ (1995) Ann Bot 75:133
6. Niklas KJ (1997a) Ann Bot 80:275
7. Niklas KJ (1997b) Ann Bot 80:437
8. Niklas KJ (1998) Ann Bot 81:11
9. Spatz HC, Speck T, Vogellehner D (1990) Bot Acta 103:123
10. Spatz HC, Boomgaarden C, Speck T (1993) Bot Acta 106:254
11. Spatz HC, Speck T (1994) Biomimetics 2:149
12. Spatz HC, Kohler L, Speck T (1998) Am J Bot 85:305
13. Speck T, Speck O, Emanns A, Spatz HC (1998) Bot Acta 111:366
14. Schulgasser K, Witztum A (1997) Ann Bot 80:35
15. Cecchini LS, Weaver PM (2002) AIAA J 40:2136
16. Corona E, Rodrigues A (1995) Comp Eng 5:163
17. Fabian O (1977) Int J Sol Struct 13:1257
18. Gerard G (1968) Minimum weight design of compressive structures. New York University Press/Interscience, New York
19. Harursampath D, Hodges DH (1999) Int J Non-Linear Mech 34:1003
20. Kedward KT (1978) In: Proceedings of the 2nd international conference on composite materials (ICCM/2). Met Soc of AIME p 353
21. Libai A, Bert CW (1994a) Int J Sol Struct 31:1003
22. Libai A, Bert CW (1994b) Int J Sol Struct 31:1019
23. NASA (1968) Space vehicles design criteria (structures)—buckling of thin-walled circular cylinders. Technical Report NASA SP-8007, NASA
24. Tatting BF, Gürdal Z, Vasiliev VV (1996) AIAA J 34:1934
25. Tatting BF, Gürdal Z, Vasiliev VV (1997) Int J Solids Struct 34:1419
26. Tsai SW, Wu EM (1971) J Comp Mater 5:58
27. Schulgasser K, Witztum A (1992) J Theor Biol 155:497
28. Brazier LG (1927) Proc Roy Soc Lond A 116:104
29. Calladine CR (1983) Theory of shell structures. Cambridge University Press, Cambridge
30. Ghavami K (1990) In: Ramanuja Rao I, Gnanaharan R, Sastry C (eds) Proceedings of the international bamboo workshop held in Cochin, India, 14–18 November. The Kerala Forest Research Institute, India and International Development Research Centre, Canada, p 235
31. Li S, Fu S, Zeng Q, Zhao X, Zhou B (1994) Biomimetics 2:15
32. Oda J (1980) Trans Japan Soc Mech Eng Ser A 46:997
33. Ueda K (1980) Res Bull Coll Exp For Hokkaido University 37:817
34. Akselrad EL (1965) Izv Akad Nauk USSR, Otdelenie Tekhnicheskikh Nauk Mech No 4:123
35. Seide P, Weingarten V (1961) J Appl Mech 28:112
36. Suo Z (1990a) J Appl Mech 57:627
37. Suo Z (1990b) Proc R Soc Lond A 427:331
38. Wegst UGK, Ashby MF (2004) Phil Mag 84:2167
39. Karam GN, Gibson JL (1995a) Int J Sol Struct 32:1259
40. Karam GN, Gibson JL (1995b) Int J Sol Struct 32:1285
41. Young WC (1989) Roark's formulas for stress and strain, 6th edn. McGraw-Hill, London
42. Mosbrugger V (1990) The tree habit in land plants. Lecture notes in Earth Sciences: 28. Springer, Berlin
43. Liese W (1985) Bamboos: biology, silvics, properties, utilization (Schriftenreihe der GTZ, Nr. 180, Deutsche Gesellschaft für Technische Zusammenarbeit (GTZ) GmbH, Dag-Hammerskjöld-Weg 1+2, D-65760 Eschborn, Germany)